

Two-dimensional superconductivity in heterostructure of titanium sesquioxide

Lijie Wang¹, Huanyi Xue¹, Guanqun Zhang¹, Zongqi Shen¹, Gang Mu², Shiwei Wu^{1,3},
Zhenghua An^{1,3}, Yan Chen¹, and Wei Li^{1,†}

¹ *State Key Laboratory of Surface Physics and Department of Physics, Fudan University, Shanghai 200433, Peoples Republic of China*

² *State Key Laboratory of Functional Materials for Informatics, Shanghai Institute of Microsystem and Information Technology, Chinese Academy of Sciences, Shanghai 200050, Peoples Republic of China*

³ *Institute for Nanoelectronic Devices and Quantum Computing, Fudan University, Shanghai 200433, Peoples Republic of China*

† Correspondence and requests for materials should be addressed to W.L. (email: w_li@fudan.edu.cn).

The search for exotic superconductivity with high-transition-temperature (T_c) in two dimensions is a central theme in condensed matter physics and materials science. Here, we report on the experimental observation of intriguing two-dimensional superconductivity with T_c of 3.8 K in the heterostructure of Mott insulator Ti_2O_3 and polar semiconductor GaN revealed by the electrical transport and magnetization measurements. Furthermore, at the verge of superconductivity we find a wide range of temperature independent resistance associated with vanishing Hall resistance, demonstrating the emergence of quantum metallic state with the Bose-metal scenario of the metallic phase. By tuning the thickness of Ti_2O_3 films, the emergence of quantum metallic state accompanies with the appearance of superconductivity as decreasing in temperature, indicating that the two-dimensional superconductivity is evolved from the quantum metallic state driven by the cooperative effects of the electron correlation and the interfacial coupling between Ti_2O_3 and polar GaN. Our work sheds new light into exploring the intriguing two-dimensional superconductivity via heterostructure engineering and promising potentials for the development of superconductor-based devices.

Heterostructure engineering represents a state-of-the-art design strategy for the realization of intriguing quantum phenomena toward the next-generation quantum technologies, because the breaking of symmetry and the particular interactions found at their interface between two constituted materials are expected to promote novel electronic phases that are not always stable as bulk phases¹⁻³. One of the most striking phenomena is the interfacial superconductivity⁴, which has been experimentally observed at the polarized interface between two band insulators $\text{LaAlO}_3/\text{SrTiO}_3$ ⁵ and the cuprate-based interface between $\text{La}_{1.55}\text{Sr}_{0.45}\text{CuO}_4$ and La_2CuO_4 ⁶, as well as the oxide-insulator/ KTaO_3 interface⁷. Besides, a prominent interface enhanced superconductivity has been reported to be above 100 K in single-layer FeSe films grown on SrTiO_3 substrate compared to the bulk FeSe displaying superconductivity below 8 K⁸⁻¹⁰, demonstrating that the electron correlation and the interface effects cooperatively contribute to the remarkable enhancement of superconductivity¹¹.

Titanium oxides are a large family of transition metal materials with many fascinating and appealing electrical properties and have potential applications as a consequence of variable oxidation states associated with strong structure-property correlations^{12,13}. Among them, titanium sesquioxide Ti_2O_3 is an antiferromagnetic Mott insulator with strong electron correlation and narrow-band gap of 0.1 eV as a result of partially filling Ti $3d^1$ band ($S=1/2$)¹⁴, which is similar to that configuration in Mott insulator LaTiO_3 ¹⁵ and promises a candidate as an unconventional superconductor driven by electron correlation effects upon charge carrier injection¹⁶. Interestingly, the transition from Mott insulating state to superconductivity has been experimentally observed on the orthorhombic phase of Ti_2O_3 films grown on $\alpha\text{-Al}_2\text{O}_3$ substrate in recent years¹⁷. The three-dimensional isotropic superconducting behavior is also revealed by angular dependent upper critical fields¹⁸. These works imply that the existence of oxygen vacancies induced electron-like charge carriers drive Mott insulator Ti_2O_3 to be a possible nontrivial superconductor with intimate correlations between structure, electrical, and magnetic properties.

In the present report, we carry out an experimental study on the Mott insulating Ti_2O_3 films grown on the polar semiconductor GaN with a wide-band gap and a high piezoelectric constant¹⁹ enabling the strong interfacial coupling effects to prompt intriguing quantum phases at their interface. The electrical transport and magnetization measurements on the as-grown films reveal the two-dimensional anisotropic superconductivity with T_c of 3.8 K. By tuning the thickness of Ti_2O_3 films, the quantum metallic state emerges accompanying with the appearance of the superconductivity as decreasing in temperature, indicating that the two-dimensional superconductivity is evolved from the quantum metallic state driven by the cooperative effects of the electron correlation and the interfacial coupling in the heterostructure of $\text{Ti}_2\text{O}_3/\text{GaN}$.

The single crystalline films of the orthorhombic phase of Ti_2O_3 (Fig. 1a) are grown on the (0001)-orientated GaN substrate with N-polar terminated face (Fig. 1b) by pulsed laser deposition. The X-ray diffraction θ - 2θ scan of the as-deposited Ti_2O_3 films at ambient conditions is used to examine these structure and phase (Fig. 1c). Apart from the GaN substrate peaks, the peaks at 37.84° and 80.85° of film with the absence of

additional peaks down to the sensitivity limit of the diffraction meter agree well with the (011) and (022) Bragg's reflection peaks of orthorhombic phase of Ti_2O_3 . The Raman spectra at ambient conditions are also used to further confirm this orthorhombic phase of Ti_2O_3 (Fig. 1d), which displays the main four peaks representing the fingerprint features of the orthorhombic Ti_2O_3 films with high structural symmetry. These results are in good agreement with that of previous reports^{17,18} and identify the structural properties of the Ti_2O_3 films grown on the GaN substrate.

Figure 2a displays the longitudinal electrical resistance R_{xx} as a function of temperature for Ti_2O_3 films measured in a Hall bar structure, schematically illustrated in the inset of Fig. 2a. The thickness of Ti_2O_3 film is 100 nm, as determined by a profilometer. The electrical resistance R_{xx} at room temperature of 300 K is 0.23 Ω . Such low electrical resistance R_{xx} implies the existence of high charge carrier concentrations and electron mobility induced by a combination of polar nature of GaN and oxygen vacancies at the interface of $\text{Ti}_2\text{O}_3/\text{GaN}$. Through the Hall effect measurements shown in Fig. 2b, the transverse Hall resistance R_{xy} reveals that the charge carriers in Ti_2O_3 film are electrons, and the carrier density is estimated to $5.67 \times 10^{16} \text{ cm}^{-2}$, approximately two orders of magnitude higher than that in $\text{LaAlO}_3/\text{SrTiO}_3$ ⁵ and EuO/KTaO_3 ⁷. The electron mobility is thus evaluated to $1208 \text{ cm}^2\text{V}^{-1}\text{s}^{-1}$ at 300 K, which is the highest values reported in the heterostructured materials thus far. At temperature lower than 200 K the sample exhibits an increase of resistance characteristic of variable range hopping-like conductivity (Fig. S2 in SI), and then saturates at a plateau of resistance with a wide temperature range of 20 K. The temperature independent electrical resistance indicates the emergence of quantum metallic state²⁰⁻²⁴, hallmark of the Bose-metal scenario of the metallic phase in the Ti_2O_3 films that a two-dimensional system of interacting bosons may form a gapless, non-superfluid state, such as a possible nature of bipolaron state resulted from the strong interfacial effect of polar GaN²⁵. In addition, the Hall resistance R_{xy} is found to be zero as a result of an inherent particle-hole symmetry²⁶ to further confirm the intrinsic behavior of this experimentally observed quantum metallic state (Fig. 2b and Fig. S3 in SI). Although qualitatively similar behavior has also been observed previously in disordered ultrathin Ga films²⁷

and gated heterostructured superconductors²⁸⁻³⁰, the origin of such quantum metallic state remains intense scrutiny²⁰⁻²². As the temperature is further decreased, it is interesting to point out that the electrical resistance R_{xx} undergoes a narrow and sharp transition width of less than 0.5 K to a zero-resistance state measured to the limit of our instrument resolution. The critical temperature is $T_c= 3.8$ K, as defined by where the resistance is a midpoint of the plateau value. The temperature dependent DC magnetization measurements with both the field-cooling (FC) and zero-field-cooling (ZFC) modes under an applied out-of-plane magnetic field of 10 Oe are also carried out to further examine the nature of zero-resistance state in Ti_2O_3 films, shown in Fig. 2c. The observed negative magnetic susceptibility that is the ratio of the measured magnetization to the applied magnetic field indicates the diamagnetism induced by the Meissner effect, unambiguously confirming the appearance of superconductivity below the T_c .

To further clarify the superconducting properties of Ti_2O_3 films, we measure the magnetoresistance $R_{xx}(\mu_0 H)$ (here μ_0 is the vacuum permeability) at various temperatures between 1.6 K and 4.4 K, with the fields perpendicular ($\mu_0 H_{\perp}$) and parallel ($\mu_0 H_{\parallel}$) to the sample plane surface, which are shown in Figs. 2d and 2e, respectively. The fundamental superconducting behaviors are clearly observed for both the superconducting critical fields $\mu_0 H_{c2}^{\perp}$ and $\mu_0 H_{c2}^{\parallel}$ that shift to a lower value with increasing temperature, where $\mu_0 H_{c2}$ is defined as the magnetic field at the midpoint of the transition in electrical resistance. It is worth pointing out that the magnetoresistance $R_{xx}(\mu_0 H)$ varies differently with $\mu_0 H_{\perp}$ and $\mu_0 H_{\parallel}$. For example, the R_{xx} as a function of $\mu_0 H_{\perp}$ reaches the normal resistance at ~ 0.25 T (the upper critical field $\mu_0 H_{c2}^{\perp}$), significantly smaller than $\mu_0 H_{c2}^{\parallel} = 1.9$ T for the parallel field at 1.6 K. This strong anisotropy in observed critical fields provides an indication of two-dimensional superconducting feature in Ti_2O_3 films. The temperature dependent upper critical fields $\mu_0 H_{c2}$ derived from the magnetoresistance $R_{xx}(\mu_0 H)$ curves in Figs. 2d and 2e are shown in Fig. 2f, and are fitted well by the phenomenological two-

dimensional Ginzburg-Landau (G-L) model³¹: $\mu_0 H_{c2}^\perp(T) = \frac{\Phi_0}{2\pi\xi_{GL}^2} \left(1 - \frac{T}{T_c}\right)$ and $\mu_0 H_{c2}^\parallel(T) = \frac{\Phi_0\sqrt{12}}{2\pi\xi_{GL}d_{SC}} \sqrt{1 - \frac{T}{T_c}}$, where Φ_0 , ξ_{GL} , and d_{SC} denote a flux quantum, the in-plane superconducting coherence length at $T = 0$ K, and the effective thickness of superconductivity, respectively. Using the extrapolated $\mu_0 H_{c2}^\perp(0) = 0.42$ T and $\mu_0 H_{c2}^\parallel(0) = 2.4$ T, we find $\xi_{GL} = 27.8$ nm and $d_{SC} = 17$ nm, suggestive of two-dimensional superconductivity in nature.

The out-of-plane polar angle (θ) dependence of the critical field H_{c2}^θ at a fixed temperature of 2 K is also carried out to further quantitatively verify the two-dimensional behavior of the superconducting Ti_2O_3 films, and shown in Fig. 3a. By projecting the magnetic fields onto the out-of-plane orientation, $H_\perp = H \cos \theta$, all the data with various values of magnetoresistance R_{xx} collapse onto a single curve, shown in Fig. 3b, suggestive of the two-dimensional characteristic of superconductivity in Ti_2O_3 films. In Fig. 3c, we also show the critical field $\mu_0 H_{c2}^\theta$ as a function of polar angle θ extracted from Fig. 3a. The data are fitted with the two-dimensional Tinkham formula (red solid curve) and the three-dimensional anisotropic G-L model (green solid curve), given by $\frac{H_{c2}^\theta |\cos \theta|}{H_{c2}^\perp} + \left(\frac{H_{c2}^\theta \sin \theta}{H_{c2}^\parallel}\right)^2 = 1$ and $\left(\frac{H_{c2}^\theta \cos \theta}{H_{c2}^\perp}\right)^2 + \left(\frac{H_{c2}^\theta \sin \theta}{H_{c2}^\parallel}\right)^2 = 1$, respectively^{32,33}. Interestingly, a cusp-like peak is clearly resolved at $\theta = 90^\circ$ and is qualitatively distinct from the three-dimensional anisotropic G-L model but is well described by the two-dimensional Tinkham model as frequently observed in interfacial superconductivity^{5,7} and layered transition metal dichalcogenides^{33,34}.

Since the superconductivity in Ti_2O_3 films grown on the GaN substrate is two-dimensional, one naturally expects fluctuations to play a crucial role and the Berezinskii-Kosterlitz-Thouless (BKT) transition to control the establishment of phase coherence^{35,36}. In this scenario, the low temperature, superconducting phase consists of bound vortex-antivortex pairs created by thermal fluctuations. On heating, the pairs dissociate and may move, inducing dissipation. The BKT temperature defines the vortex unbinding transition and can be determined using current-voltage (I - V) measurements as a function of temperature T , as shown in Fig. 3d. Below T_c we find a

clear critical current I_c , whose value decreases with increasing measurement temperature. This is further evidence for the existence of superconductivity in Ti_2O_3 films. The maximal value of I_c is ~ 15 mA at 1.6 K, which is approximately more than two orders of magnitude higher than that observed in EuO/KTaO_3 ⁷ and $\text{LaAlO}_3/\text{KTaO}_3$ ³⁷, and more than three orders of magnitude higher than that observed in $\text{LaTiO}_3/\text{SrTiO}_3$ ³⁸ and $\text{LaAlO}_3/\text{SrTiO}_3$ ⁵. Such significantly higher critical current value is a resultant from the high charge carrier concentrations of $5.67 \times 10^{16} \text{ cm}^{-2}$ in Ti_2O_3 films, promising for large scale applications in superconductor-based devices. In Fig. 3e, we plot the I - V on a log-log scale and observe that slope of the I - V characteristics evolves smoothly from the normal ohmic state, $V \propto I$, toward a steeper power law resulting from that the current excites free-moving vortices, $V \propto I^{\alpha(T)}$, as superconductivity sets in at lower temperatures. At T_{BKT} , a two-dimensional superconductor obeys the universal scaling relation, $V \propto I^3$. In Fig. 3f, we plot α versus T , as determined by the slope of the different V - I traces on a log-log scale shown in Fig. 3e, and determine $T_{\text{BKT}} = 3.3$ K from where $\alpha = 3$ interpolates, only slightly less than T_c as defined in Fig. 2a. In addition, close to T_{BKT} , a $R_{\text{sheet}} = R_0 \exp[-b(T/T_{\text{BKT}} - 1)^{-1/2}]$ dependence, where R_0 and b are material parameters, is expected³⁹. As shown in Fig. 3g, the measured $R_{\text{sheet}}(T)$ is consistent with this behavior and yields $T_{\text{BKT}} = 3.75$ K, in good agreement with the analysis of the α exponent. Therefore, the superconducting transition of the heterostructure of $\text{Ti}_2\text{O}_3/\text{GaN}$ is consistent with that of a two-dimensional superconducting film.

To further shed light on the nature of two-dimensional superconductivity and its intriguing relation to the quantum metallic state in the heterostructure of $\text{Ti}_2\text{O}_3/\text{GaN}$, we carry out the measurements of thickness dependent superconductivity in Ti_2O_3 films ranging from 6 nm to 108 nm. As shown in Fig. 4a, we find that the thinner film of Ti_2O_3 with thickness of 6 nm displays an insulating behavior. When the sample thickness increases, the electrical resistance decreases and saturates at the lowest temperature. If we further increase the thickness of sample, the heterostructures of $\text{Ti}_2\text{O}_3/\text{GaN}$ undergo a transition from insulator to superconductivity accompanying with

the appearance of the quantum metallic state with the indications of the temperature independent resistance and vanished Hall resistance as decreasing in temperature (Fig. 4a and 4b). The T_c increases with thickness and saturates at 3.8 K when the thickness is larger than 95 nm, as shown in Fig. 4a. The thickness independent T_c in the thicker films provides further strong evidence for the interface superconductivity. These results indicate that the two-dimensional superconductivity at the interface of $\text{Ti}_2\text{O}_3/\text{GaN}$ is evolved from the quantum metallic state as decreasing in temperature driven by cooperative effects of the electron correlation and the interfacial coupling between Ti_2O_3 films and polar GaN (see the phase diagram in Fig. 4c). Consistent results have also been observed on all our thin films, and these results are highly reproducible, demonstrating that these experimental findings are an intrinsic property of the superconductivity at their interface of $\text{Ti}_2\text{O}_3/\text{GaN}$. The origin of this two-dimensional superconductivity and the quantum metallic state, however, remains elusive. Further experiments, including probes of temperature dependent microscopic electronic state evolutions at the interface and the spatial structure of superconductivity, will be helpful for elucidating the nature of these intriguing quantum states that we observe. Therefore, an exotic interface superconductivity with unusual electronic properties including high T_c of 3.8 K, high critical current I_c of 15 mA, and high sheet charge carrier concentrations of $5.67 \times 10^{16} \text{ cm}^{-2}$ and large electron mobility of $1208 \text{ cm}^2\text{V}^{-1}\text{s}^{-1}$ at 300 K, is experimentally observed in the heterostructure of strongly correlated Mott insulator Ti_2O_3 and polar semiconductor GaN, which not only opens a new platform to clarify the intriguing two-dimensional superconductivity with a delicate interplay of interfacial coupling and the strong electron correlation and to further unveil the clues of the mechanism of unconventional superconductivity, but also provides a unique opportunity for developing the next-generation quantum technologies.

Materials and Methods

Thin films growth and structural characterization. The Ti_2O_3 thin films are grown on the GaN (0001) substrates by pulsed laser deposition in an ultrahigh-vacuum chamber (base pressure of 10^{-7} Torr). Prior to growth, the GaN substrates are ultrasonically cleaned with acetone and ethanol. During the deposition, the sintered Ti_2O_3 ceramic target (Kurt J. Lesker Company Inc.) is used to grow the Ti_2O_3 films with a KrF excimer laser (Coherent 102, wave-length: $\lambda = 248$ nm). The pulse energy of 110 mJ and repetition rate of 10 Hz are used. The Ti_2O_3 films are deposited at 750 °C in a vacuum chamber to promote growth of the superconducting phase [also see the patterns of reflection high energy diffraction shown in Fig. S1 in supplementary information (SI)]. All the samples are cooled down to room temperature at a constant rate of 20 °C/min in vacuum after deposition. The crystalline quality of Ti_2O_3 films at ambient conditions are examined by X-ray diffraction using the BL02U2 beamline of the Shanghai Synchrotron Radiation Facility (SSRF) with an X-ray wavelength of 0.886Å, and by Raman measurements using a confocal micro-Raman system (Horiba Jobin Yvon HR-Evolution 2) with the wavelength of the excitation solid-state laser of 532nm. The thickness of Ti_2O_3 films is measured by using a stylus profilometer (Bruker DektakXT).

Magnetization and electrical transport measurements. Before the electrical transport measurements, the magnetic properties of the Ti_2O_3 films are measured using the superconducting quantum interference devices (SQUID) magnetometer (MPMS, Quantum Design Inc.). For measurements of the direct current (DC) magnetization as a function of temperature, the samples are first cooled down to 2 K in zero field and then out-of-plane magnetic field of 10 Oe is applied. The magnetization data are collected during warming up from 2 K to 15 K (ZFC: zero-field cooled process). In the same fixed field, the samples are then cooled down to 2 K again and the magnetization data are recollected during warming up from 2 K to 15 K (FC: field-cooled process). The electrical transport measurements are performed using in a cryostat (Oxford Instruments TeslatronPT cryostat system). The Hall bar structure, schematically

illustrated in inset of Fig. 2a, is fabricated by using the technique of ion-beam etching to measure the electrical transport properties.

Reference

1. Mannhart, J. & Schlom, D. G. Oxide interfaces—An opportunity for electronics. *Science* **327**, 1607-1611 (2010).
2. Zubko, P. *et al.* Interface physics in complex oxide heterostructures. *Annu. Rev. Condens. Matter Phys.* **2**, 141-165 (2011).
3. Hwang, H. Y. *et al.* Emergent phenomena at oxide interfaces. *Nature Materials* **11**, 103-113 (2012).
4. Saito, Y., Nojima, T., & Iwasa, Y. Highly crystalline 2D superconductors. *Nature Reviews Materials* **2**, 16094 (2017).
5. Reyren, N. *et al.* Superconducting interfaces between insulating oxides. *Science* **317**, 1196-1199 (2007).
6. Gozar, A. *et al.* High-temperature interface superconductivity between metallic and insulating copper oxides. *Nature* **455**, 782-785 (2008).
7. Liu, C. *et al.* Two-dimensional superconductivity and anisotropic transport at KTaO₃ (111) interfaces. *Science* **371**, 716-721 (2021).
8. Wang, Q. *et al.* Interface-induced high-temperature superconductivity in single unit-cell FeSe films on SrTiO₃. *Chin. Phys. Lett.* **29**, 037402 (2012).
9. Ge, J. *et al.* Superconductivity above 100 K in single-layer FeSe films on doped SrTiO₃. *Nature Materials* **14**, 285-289 (2015).
10. Hsu, F. *et al.* Superconductivity in the PbO-type structure α -FeSe. *Proc. Natl. Acad. Sci. U. S.A.* **105**, 14262–14264 (2008).
11. Lee, J. J. *et al.* Interfacial mode coupling as the origin of the enhancement of T_c in FeSe films on SrTiO₃. *Nature* **515**, 245–248 (2014).
12. Jeong, D. S. *et al.* Emerging memories: resistive switching mechanisms and current status. *Rep. Prog. Phys.* **75**, 076502 (2012).
13. Yang, J. J., Strukov, D. B., & Stewart, D. R. Memristive devices for computing. *Nat. Nanotechnol.* **8**, 13–24 (2013).
14. Morin, F. J. Oxides which show a metal-to-insulator transition at the Neel temperature. *Phys. Rev. Lett.* **3**, 34 (1959).
15. Keimer, B. *et al.* Spin Dynamics and Orbital State in LaTiO₃. *Phys. Rev. Lett.* **85**, 3946 (2000).
16. Li, Y. *et al.* Orthorhombic Ti₂O₃: A polymorph-dependent narrow-bandgap ferromagnetic oxide. *Adv. Funct. Mater.* **28**, 1705657 (2018).

17. Li, Y. *et al.* Observation of superconductivity in structure-selected Ti₂O₃ thin films. *NPG Asia Materials* **10**, 522–532 (2018).
18. Feng, J. *et al.* Phase evolution with the film thickness in PLD-grown titanium oxides films. *Journal of Alloys and Compounds* **831**, 154727 (2020).
19. Bernardini, F., Fiorentini, V., & Vanderbilt, D. Spontaneous polarization and piezoelectric constants of III-V nitrides. *Phys. Rev. B* **56**, R10024 (1997).
20. Kapitulnik, A., Kivelson, S. A., & Spivak, B. Anomalous metals: Failed superconductors. *Rev. Mod. Phys.* **91**, 011002 (2019).
21. Fisher, M. P. A. *et al.* Boson localization and the superfluid-insulator transition. *Phys. Rev. B* **40**, 546 (1989).
22. Phillips, P. & Dalidovich, D. The elusive Bose metal. *Science* **302**, 243-247 (2003).
23. Saito, Y. *et al.* Metallic ground state in an ion-gated two-dimensional superconductor. *Science* **350**, 409-413 (2015).
24. Tsen, A. W. *et al.* Nature of the quantum metal in a two-dimensional crystalline superconductor. *Nature Physics* **12**, 208–212 (2016).
25. Alexandrov, A. S. & Mott, S. N. *Polarons and Bipolarons* (World Scientific, Singapore, 1995).
26. Breznay, N. P. & Kapitulnik, A. Particle-hole symmetry reveals failed superconductivity in the metallic phase of two-dimensional superconducting films. *Sci. Adv.* **3**, e1700612 (2017).
27. Christiansen, C., Hernandez, L. M., & Goldman, A. M. Evidence of collective charge behavior in the insulating state of ultrathin films of superconducting metals. *Phys. Rev. Lett.* **88**, 037004 (2002).
28. Biscaras, J. *et al.* Two-dimensional superconducting phase in LaTiO₃/SrTiO₃ heterostructures induced by high-mobility carrier doping. *Phys. Rev. Lett.* **108**, 247004 (2012).
29. Chen, Z. *et al.* Carrier density and disorder tuned superconductor-metal transition in a two-dimensional electron system. *Nature Communications* **9**, 4008 (2018).
30. Chen, Z. *et al.* Electric field control of superconductivity at the LaAlO₃/KTaO₃(111) interface. *Science* **372**, 721-724 (2021).
31. Tinkham, M. *Introduction to Superconductivity*; 2nd edn (McGraw-Hill, New York, 1996).
32. Tinkham, M. Effect of fluxoid quantization on transitions of superconducting films. *Phys. Rev.* **129**, 2413 (1963).

33. Lu, J. M. *et al.* Evidence for two-dimensional Ising superconductivity in gated MoS₂. *Science* **350**, 1353–1357 (2015).
34. Jiang, D. *et al.* Strong in-plane magnetic field-induced reemergent superconductivity in the van der Waals heterointerface of NbSe₂ and CrCl₃. *ACS Appl. Mater. Interfaces* **12**, 49252–49257 (2020).
35. Kosterlitz, J. M. & Thouless, D. J. Long range order and metastability in two dimensional solids and superfluids. *J. Phys. Chem.* **5**, L124–L126 (1972).
36. Beasley, M. R., Mooij, J. E., & Orlando, T. P. Possibility of vortex-antivortex pair dissociation in two-dimensional superconductors. *Phys. Rev. Lett.* **42**, 1165 (1979).
37. Chen, Z. *et al.* Two-dimensional superconductivity at the LaAlO₃/KTaO₃ (110) heterointerface. *Phys. Rev. Lett.* **126**, 026802 (2021).
38. Biscaras, J. *et al.* Two-dimensional superconductivity at a Mott insulator/band insulator interface LaTiO₃/SrTiO₃. *Nature Communications* **1**, 89 (2010).
39. Halperin, B. I. & Nelson, D. R. Resistive transition in superconducting films. *J. Low Temp. Phys.* **36**, 599–616 (1979).

Acknowledgments

This work was supported by the National Natural Science Foundation of China (Grant No. 11927807) and Shanghai Science and Technology Committee (Grant Nos. 18JC1420400 and 20DZ1100604). The authors thanked beamline BL02U2 of Shanghai Synchrotron Radiation Facility.

Author contributions

W.L. conceived the project and designed the experiments. L.W. grown the samples and performed the measurements. H.X. and Z.A. fabricated the Hall bar structure on the thin films. All the authors discussed the results. W.L. wrote the paper. L.W. and W.L. revised the paper.

Author Information

The authors declare no competing financial interests. Correspondence and requests for materials should be addressed to W.L. (email: w_li@fudan.edu.cn).

Fig. 1

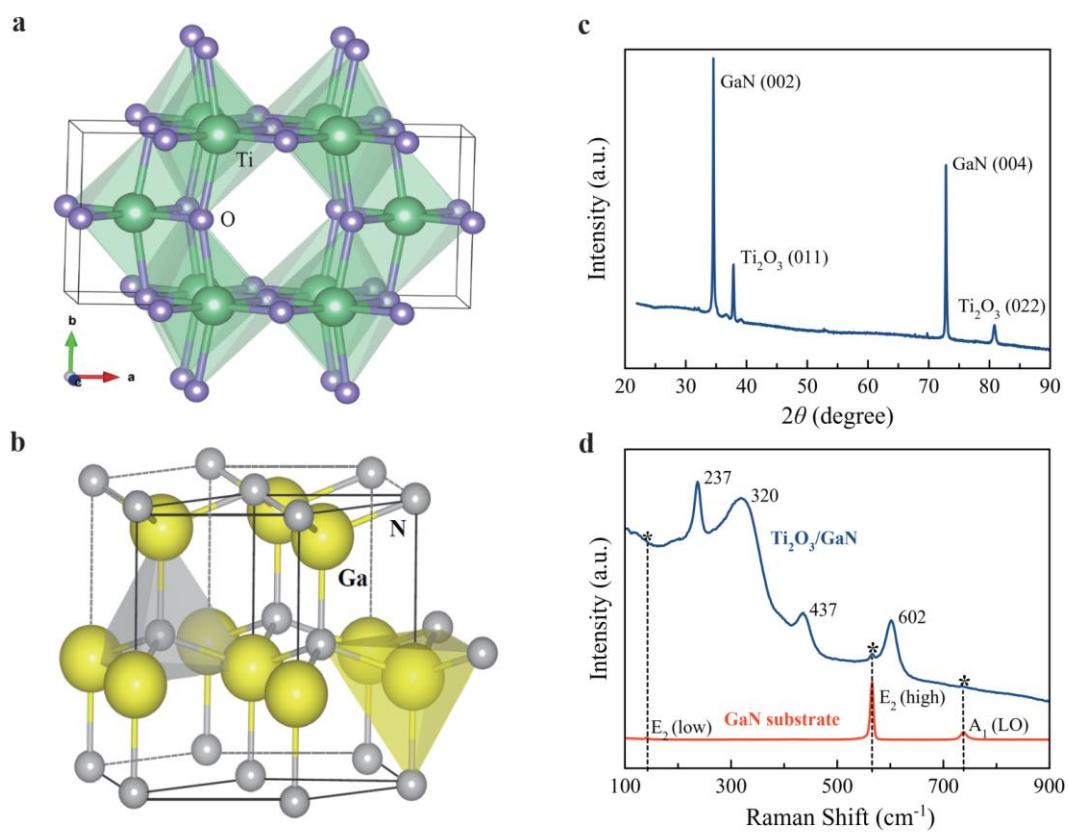


Fig. 1. Structural properties of $\text{Ti}_2\text{O}_3/\text{GaN}$ at ambient conditions. a, Crystal structure of orthorhombic phase of Ti_2O_3 . **b**, Crystal structure of polar semiconductor GaN. **c**, High-resolution X-ray diffraction θ - 2θ spectra of the Ti_2O_3 films grown on GaN (0001) substrate. **d**, Raman spectra of $\text{Ti}_2\text{O}_3/\text{GaN}$ and GaN substrate with wavelength of excitation laser of 532 nm.

Fig. 2

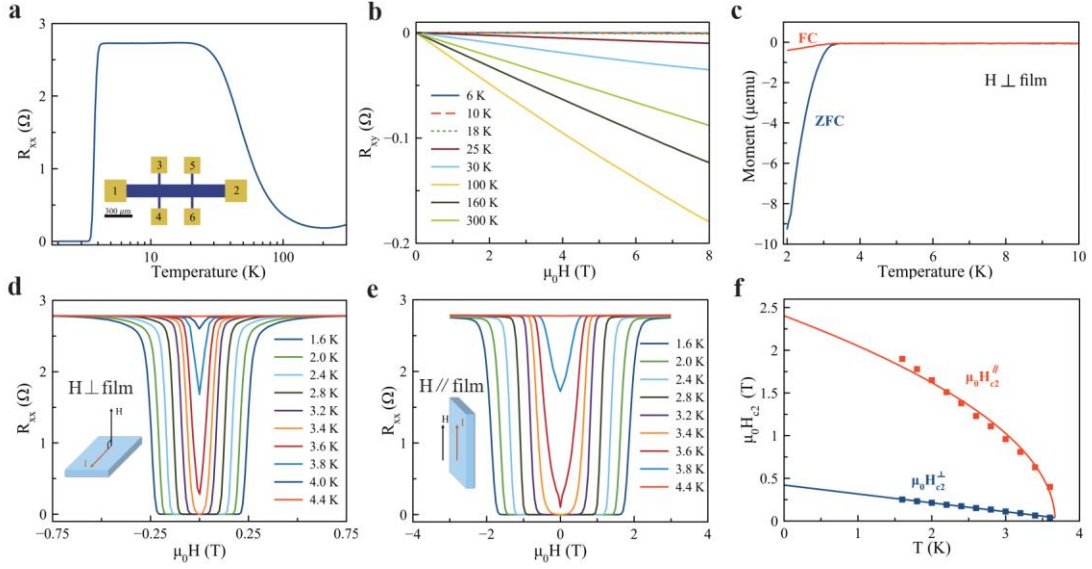


Fig. 2. Electronic properties of Ti₂O₃/GaN. **a**, Temperature dependence of the longitudinal electrical resistance R_{xx} at zero magnetic field for Ti₂O₃/GaN. The Hall bar structure is schematically illustrated in the inset of figure (a). **b**, Transverse Hall resistance R_{xy} versus out-of-plane magnetic field with fixed various temperatures. **c**, Temperature dependence of the DC magnetization of Ti₂O₃/GaN in FC and ZFC modes with an applied out-of-plane magnetic field of 10 Oe. Magnetoconductance for fields **d**, perpendicular and **e**, parallel to the sample plane surface. **f**, Temperature dependence of upper critical fields $\mu_0 H_{c2}$, which are determined at the half of values of R_{xx} in (d) and (e), respectively.

Fig. 3

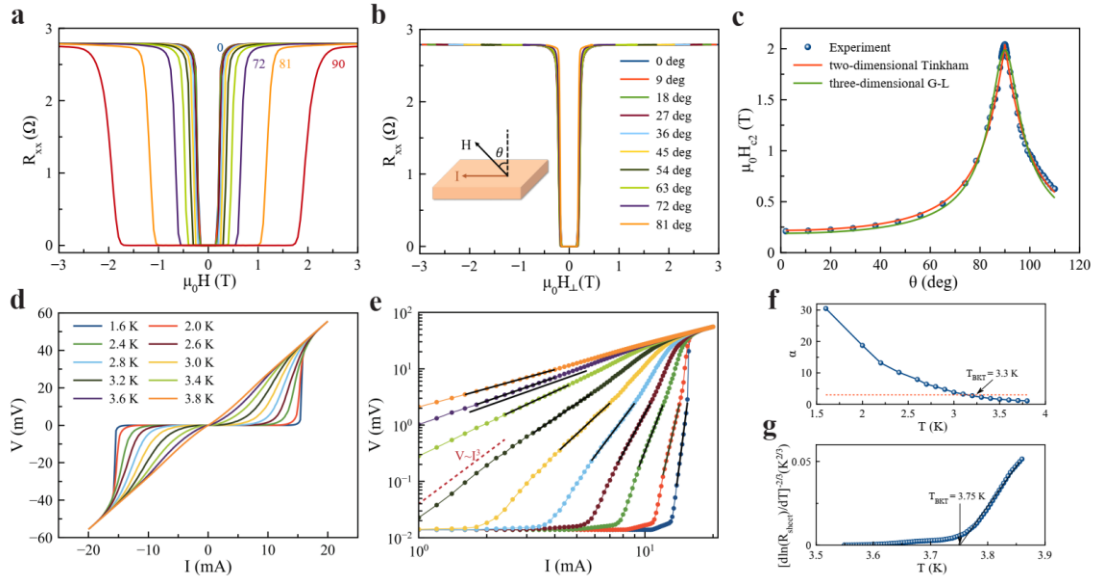


Fig. 3. Two-dimensional superconducting behaviors of $\text{Ti}_2\text{O}_3/\text{GaN}$. **a**, Longitudinal electrical resistance R_{xx} as a function of the strength of magnetic field at various polar angle values θ ranging from $\theta = 0^\circ$ to 90° at a fixed temperature of 2 K. **b**, The corresponding R_{xx} in (a) after the projection of the magnetic field into the out-of-plane orientation. **c**, Critical field $\mu_0 H_{c2}^\theta$ as a function of polar angle θ . The red and green solid lines are fitted to the data using the two-dimensional Tinkham model and three-dimensional G-L model, respectively. **d**, Temperature dependent I - V measurements. **e**, The corresponding logarithmic scale in (d). The long red dashed line denotes the $V \sim I^3$ dependence. **f**, Temperature dependence of the power-law exponent α , as deduced from the fits shown in (e). **g**, $R_{\text{sheet}}(T)$ dependence of the same sample, plotted on a $[d \ln(R_{\text{sheet}})/dT]^{-2/3}$ scale. The solid line is the behavior expected for a BKT transition with $T_{\text{BKT}} = 3.75$ K.

Fig. 4

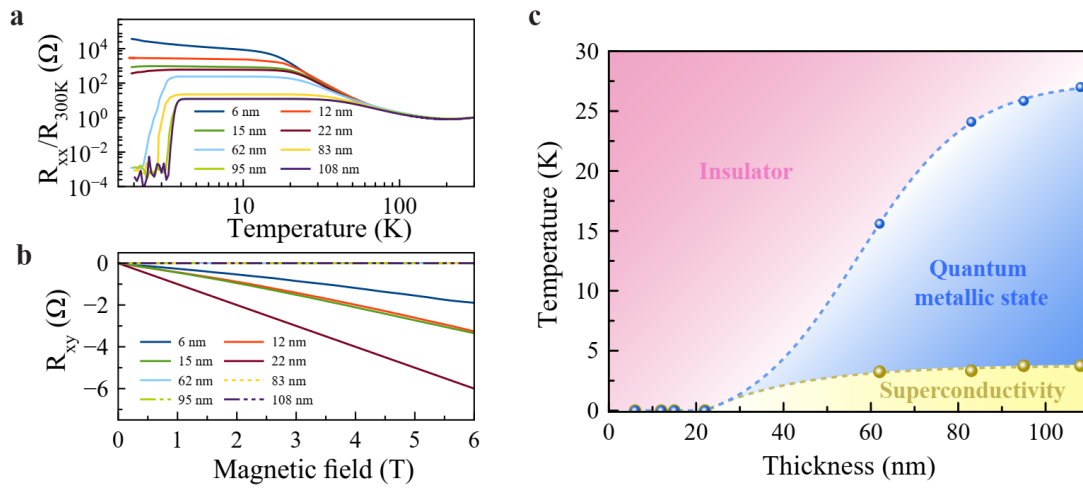


Fig. 4. The thickness dependent superconductivity in $\text{Ti}_2\text{O}_3/\text{GaN}$. **a**, Thickness dependence of the rescaled electrical resistance R_{xx} as a function of temperature. The $R_{300\text{K}}$ denotes the electrical resistance measured at a temperature of 300 K. **b**, Thickness dependence of the transverse Hall resistance R_{xy} with respect to the applied field $\mu_0 H$ at the temperature of 18 K. **c**, Thickness dependent phase diagram of $\text{Ti}_2\text{O}_3/\text{GaN}$ including the phases of insulator, quantum metallic state, and the superconductivity.